J Mater Sci (2009) 44:4883–4891
DOI 10.1007/s10853-009-3746-7

Investigation of the quasi-ternary system $LaMnO_3$–$LaCoO_3$–"$LaCuO_3$". II: The series $LaMn_{0.25-x}Co_{0.75-x}Cu_{2x}O_{3-\delta}$ and $LaMn_{0.75-x}Co_{0.25-x}Cu_{2x}O_{3-\delta}$

F. Tietz · I. Arul Raj · Q. X. Fu · M. Zahid

Received: 23 January 2009 / Accepted: 15 July 2009 / Published online: 31 July 2009

Abstract This paper investigates the crystal structure, thermal expansion, and electrical conductivity of two series of perovskites ($LaMn_{0.25-x}Co_{0.75-x}Cu_{2x}O_{3-\delta}$ and $LaMn_{0.75-x}Co_{0.25-x}Cu_{2x}O_{3-\delta}$ with $x = 0$, 0.025, 0.05, 0.1, 0.15, 0.2, and 0.25) in the quasi-ternary system $LaMnO_3$–$LaCoO_3$–"$LaCuO_3$". The Mn/Co ratio was found to have a stronger influence on these properties than the Cu content. In comparison to the Co-rich series ($LaMn_{0.25-x}Co_{0.75-x}Cu_{2x}O_{3-\delta}$), the Mn-rich series ($LaMn_{0.75-x}Co_{0.25-x}Cu_{2x}O_{3-\delta}$) showed a much higher Cu solubility. All compositions in this series were single-phase materials after calcination at 1100 °C. The Co-rich series showed higher thermal expansion coefficients ($\alpha_{max} = 19.6 \times 10^{-6}$ K^{-1}) and electrical conductivity ($\sigma_{max} = 730$ S/cm at 800 °C) than the Mn-rich series ($\alpha_{max} = 10.6 \times 10^{-6}$ K^{-1}, $\sigma_{max} = 94$ S/cm at 800 °C). Irregularities in the thermal expansion curves indicated phase transitions at 150–350 °C for the Mn-rich series, while partial melting occurred at 980–1000 °C for the Co-rich series with $x > 0.15$.

I. Arul Raj—on leave from Central Electrochemical Research Institute, Karaikudi, 630006 India.

F. Tietz (✉) · I. Arul Raj · Q. X. Fu · M. Zahid
Institut für Energieforschung (IEF-1), Forschungszentrum Jülich, 52425 Jülich, Germany
e-mail: f.tietz@fz-juelich.de

Present Address:
Q. X. Fu · M. Zahid
European Institute for Energy Research (EIfER), Emmy-Noether-Strasse 11, 76131 Karlsruhe, Germany

Introduction

Perovskite-type oxides, especially $LaMeO_{3-\delta}$ with Me = Cr, Mn, Fe, Co, Ni, Cu, have been investigated by many research groups because of their interesting electrical, magnetic, and oxygen transport properties which makes them suitable for application as functional materials in solid oxide fuel cells or as giant magnetoresistant materials. In order to tailor the properties for a certain application, elemental substitution at A-sites or B-sites of the perovskite lattice is often used as this forms complex perovskite-type oxides. For instance, complex oxides in the system $LaMnO_3$–$LaCoO_3$ have been widely investigated in terms of their crystal structure, electrical and ionic conductivity, catalytic, magnetic and thermal expansion behavior [1–10]. Crystallographic studies have also been conducted on $LaCoO_3$–$LaCuO_3$ and $LaMnO_3$–$LaCuO_3$ systems [11–13]. As far as we know, however, systematic studies on the complex system of $LaMnO_3$–$LaCoO_3$–$LaCuO_3$ have not yet been performed.

In our previous study, the sintering behavior and properties of the oxides in the series $La(Mn_{0.5}Co_{0.5})_{1-x}Cu_xO_{3-\delta}$ with $x = 0$, 0.05, 0.1, 0.2, 0.4, 0.6, 0.8, and 1 were investigated and the results were reported as the first part of investigations into this complex system [14]. Some remarkable results were obtained along this series of perovskite compositions: $LaMn_{0.3}Co_{0.3}Cu_{0.4}O_{3-\delta}$ crystallized as a single phase with an orthorhombic perovskite structure. Among the synthesized compositions, this compound showed the highest electrical conductivity in air at 800 °C (155 S cm^{-1}) and the highest thermal expansion coefficient ($\alpha_{30-800\ °C} = 15.4 \times 10^{-6}$ K^{-1}). The "$LaCuO_{3-\delta}$" composition crystallized as a mixture of La_2CuO_4 and CuO at 900 °C and as a single phase with a monoclinic $La_2Cu_2O_5$-type structure at 1100 °C, although previous

investigations have shown that other phases are preferably formed [15, 16].

For this study, perovskites with different Mn/Co ratio were prepared and systematically characterized, i.e. seven oxides in the series $LaMn_{0.25-x}Co_{0.75-x}Cu_{2x}O_{3-\delta}$ and another seven oxides in the series $LaMn_{0.75-x}Co_{0.25-x}Cu_{2x}O_{3-\delta}$ with $x = 0$, 0.025, 0.05, 0.1, 0.15, 0.2, and 0.25 for both series. The X-ray crystallographic data, the thermal expansion coefficient data, and the electrical conductivity data were obtained on sintered samples fabricated from these oxide powders and compared as a function of the copper content.

Experimental

Fourteen powders with different compositions within the series $LaMn_{0.25-x}Co_{0.75-x}Cu_{2x}O_{3-\delta}$ and $LaMn_{0.75-x}Co_{0.25-x}Cu_{2x}O_{3-\delta}$ (both with $x = 0$, 0.025, 0.05, 0.1, 0.15, 0.2, and 0.25) were synthesized by the Pechini method [17] using nitrate solutions of La, Mn, Co, and Cu in the corresponding metallic ratios. A detailed description of the synthesis process is given in Ref. [18]. After obtaining the raw powder and calcination at 600 °C for 3 h, the powders were subjected to chemical analysis using inductively coupled plasma with optical emission spectroscopy (ICP-OES, TJA-IRIS-INTREPID spectrometer) to confirm the nominal stoichiometry. In addition, two samples of each prepared powder were heat-treated in air at 900 and 1100 °C for 6 h. The crystal phase composition of these samples was determined by X-ray diffraction analysis using a Siemens D5000 diffractometer with CuK_{α} radiation. Lattice parameters and contents of secondary phases were determined by Rietveld refinement.

The powders calcined at 600 °C were uniaxially pressed to bars ($40 \times 5 \times 4$ mm^3) and sintered at either 1300 °C (for $x \leq 0.15$) or 1100 °C (for $x \geq 0.2$) for 6 h in air. Densities of sintered samples were measured by the Archimedean method. The thermal expansion between 30 and 800 °C was determined using a Netzsch DIL 402C dilatometer. The total electrical conductivity of the sintered samples was measured by a 4-probe DC technique at temperatures between 100 and 900 °C in air using silver wires and silver paste as contacts.

Results and discussion

Elemental analysis of the powders

Considering the precision limit (1–3%) of the analytical technique used (ICP-OES), no considerable deviations were observed between the analytical and the nominal compositions of the synthesized powders (Table 1).

Crystallography

For all powders in the series $LaMn_{0.25-x}Co_{0.75-x}Cu_{2x}O_{3-\delta}$ calcined at 900 or 1100 °C, in addition to the main perovskite phase, small amounts or traces of minor phases were also observed, as shown in Fig. 1. The main phase for all powders had a rhombohedral perovskite structure (P_{rh}) similar to $LaCoO_3$ (space group $R\,\bar{3}\,c$, JCPDS file no. 48-123). After calcination at 900 °C, La_2O_3 and Co_3O_4

Table 1 Nominal composition, analytical composition, and crystalline phases observed after calcination at 900 °C and 1100 °C for 6 h

Nominal composition	Analytical composition	Crystalline phases (numbers in parentheses indicate the phase content in wt%)	
		900 °C	1100 °C
$LaMn_{0.25}Co_{0.75}O_{3-\delta}$	$La_{1.02}Mn_{0.25}Co_{0.74}O_{3-\delta}$	$P_{rh} + La_2O_3 + Co_3O_4$	$P_{rh} + La_2O_3$ (1) + Co_3O_4 (1)
$LaMn_{0.225}Co_{0.725}Cu_{0.05}O_{3-\delta}$	$La_{1.00}Mn_{0.22}Co_{0.72}Cu_{0.05}O_{3-\delta}$	$P_{rh} + La_2O_3 + Co_3O_4$	$P_{rh} + La_2O_3$ (1) + Co_3O_4 (3)
$LaMn_{0.20}Co_{0.70}Cu_{0.10}O_{3-\delta}$	$La_{1.01}Mn_{0.20}Co_{0.69}Cu_{0.10}O_{3-\delta}$	$P_{rh} + La_2O_3$ + L2C + Co_3O_4	P_{rh} + L2C (3)
$LaMn_{0.15}Co_{0.65}Cu_{0.20}O_{3-\delta}$	$La_{1.00}Mn_{0.15}Co_{0.65}Cu_{0.21}O_{3-\delta}$	P_{rh} + L2C + La_2O_3 + Co_3O_4	P_{rh} + L2C (1)
$LaMn_{0.10}Co_{0.60}Cu_{0.30}O_{3-\delta}$	$La_{1.02}Mn_{0.10}Co_{0.58}Cu_{0.31}O_{3-\delta}$	P_{rh} + L2C	P_{rh} + L2C (3)
$LaMn_{0.05}Co_{0.55}Cu_{0.40}O_{3-\delta}$	$La_{1.00}Mn_{0.05}Co_{0.54}Cu_{0.41}O_{3-\delta}$	P_{rh} + L2C	P_{rh} + L2C2 (2) + L2C (7)
$LaCo_{0.50}Cu_{0.50}O_{3-\delta}$	$La_{1.00}Co_{0.49}Cu_{0.52}O_{3-\delta}$	P_{rh} + L2C + CuO	P_{rh} + L2C2 (22) + L2C (2)
$LaMn_{0.75}Co_{0.25}O_{3-\delta}$	$La_{1.01}Mn_{0.74}Co_{0.25}O_{3-\delta}$	P_{or}	P_{or}
$LaMn_{0.725}Co_{0.225}Cu_{0.05}O_{3-\delta}$	$La_{1.01}Mn_{0.71}Co_{0.22}Cu_{0.05}O_{3-\delta}$	P_{or}	P_{or}
$LaMn_{0.70}Co_{0.20}Cu_{0.10}O_{3-\delta}$	$La_{1.02}Mn_{0.68}Co_{0.20}Cu_{0.10}O_{3-\delta}$	P_{or}	P_{or}
$LaMn_{0.65}Co_{0.15}Cu_{0.20}O_{3-\delta}$	$La_{1.01}Mn_{0.64}Co_{0.14}Cu_{0.21}O_{3-\delta}$	P_{or}	P_{or}
$LaMn_{0.60}Co_{0.10}Cu_{0.30}O_{3-\delta}$	$La_{1.00}Mn_{0.59}Co_{0.10}Cu_{0.32}O_{3-\delta}$	P_{or}	P_{or}
$LaMn_{0.55}Co_{0.05}Cu_{0.40}O_{3-\delta}$	$La_{1.01}Mn_{0.52}Co_{0.05}Cu_{0.42}O_{3-\delta}$	P_{or} + L2C	P_{or}
$LaMn_{0.50}Cu_{0.50}O_{3-\delta}$	$La_{1.00}Mn_{0.49}Cu_{0.51}O_{3-\delta}$	P_{or} + L2C	P_{or}

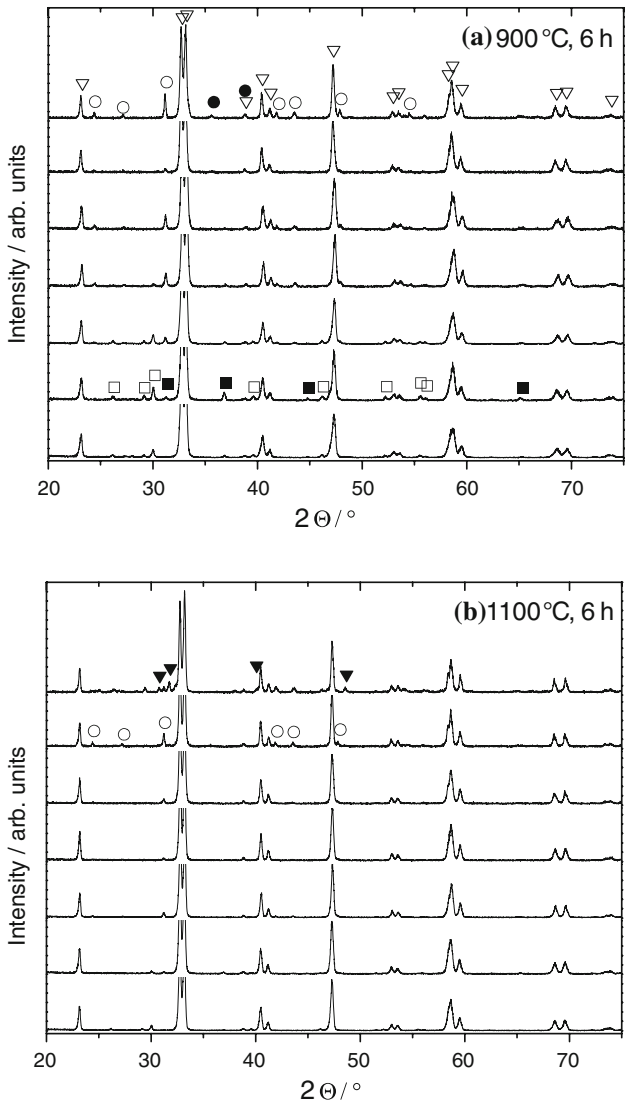

Fig. 1 XRD patterns of $LaMn_{0.25-x}Co_{0.75-x}Cu_{2x}O_{3-\delta}$ ($x = 0$, 0.025, 0.05, 0.1, 0.15, 0.2, and 0.25, from bottom to top) after heat treatment at **a** 900 °C and **b** 1100 °C for 6 h. The main phase with a rhombohedral perovskite structure (P_{rh}) is indicated with *open triangles*. The formation of minor phases is also indicated with different symbols. *Open squares*: La_2O_3; *closed squares*: Co_3O_4; *open circles*: La_2CuO_4; *closed circles*: CuO; *closed triangles*: $La_2Cu_2O_5$

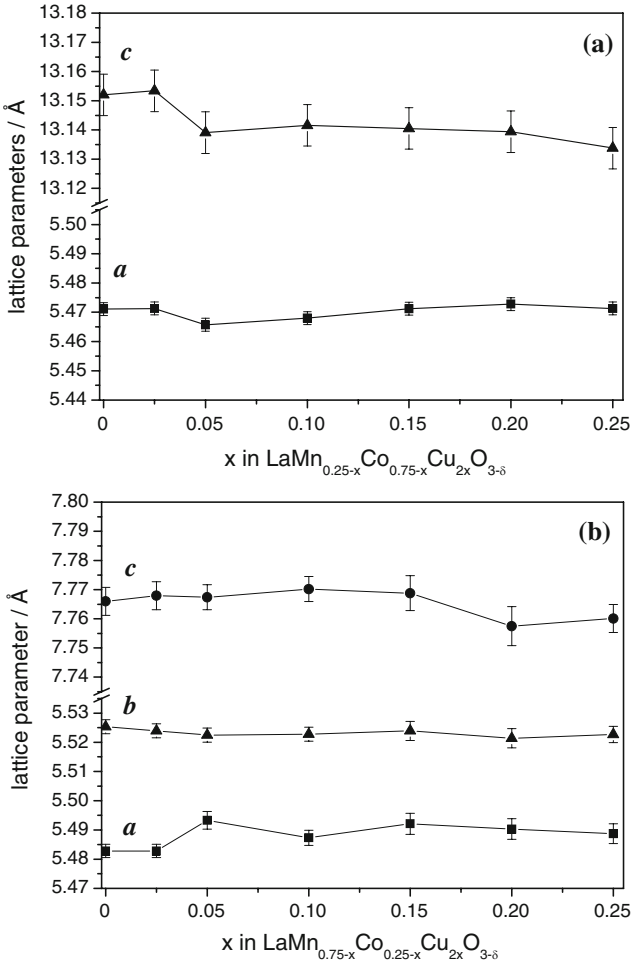

Fig. 2 Lattice parameters of the series $LaMn_{0.25-x}Co_{0.75-x}Cu_{2x}O_{3-\delta}$ (**a**) and $LaMn_{0.75-x}Co_{0.25-x}Cu_{2x}O_{3-\delta}$ (**b**) after sintering at 1100 °C

were detected as minor phases for $x = 0$ and $x = 0.025$. With increasing Cu content ($x \geq 0.05$), La_2CuO_4 (L2C, space group *Fmmm*, JCPDS file no. 38-709) appeared as a minor phase. The end member $LaCu_{0.50}Co_{0.50}O_{3-\delta}$ contained a significant amount of La_2CuO_4 and consequently CuO was also detected. The coexistence of La_2O_3 and Co_3O_4 in compositions with $x \leq 0.1$ indicates an incomplete reaction at 900 °C, which is supported by a reduced amount of these two phases after calcination at 1100 °C. For $x \geq 0.05$, the La_2CuO_4 phase remained as the minor phase after calcination at 1100 °C with amounts of $\leq$7 wt% (see Table 1). For the end member $LaCu_{0.50}Co_{0.50}O_{3-\delta}$ calcined at 1100 °C, the $La_2Cu_2O_5$ phase (L2C2, space group *C2/c*, JCPDS file no. 45-10) was additionally detected with a significant amount. This result is in agreement with our previous work on the series $La(Mn_{0.5}Co_{0.5})_{1-x}Cu_xO_{3-\delta}$ [14], where La_2CuO_4 and CuO formed at 900 °C tended to transform to $La_2Cu_2O_5$ at 1100 °C.

The lattice parameters of the samples sintered at 1100 °C are shown in Fig. 2a. Due to the additional phases formed (Table 1), the data are not meaningful for discussing the dependence of the lattice parameters on substitution with Cu. However, in accordance with the appearance of L2C as an impurity, the lattice parameters *a* and *c* show a sudden drop between $x = 0.025$ and 0.05, indicating the solubility limit of Cu in $LaMn_{0.25-x}Co_{0.75-x}Cu_{2x}O_{3-\delta}$.

For $LaMn_{0.75-x}Co_{0.25-x}Cu_{2x}O_{3-\delta}$ calcined at 900 °C, single-phase orthorhombic perovskites (P_{or}) similar to $LaMnO_3$ (space group *Pnma*, JCPDS file no. 89-2470)

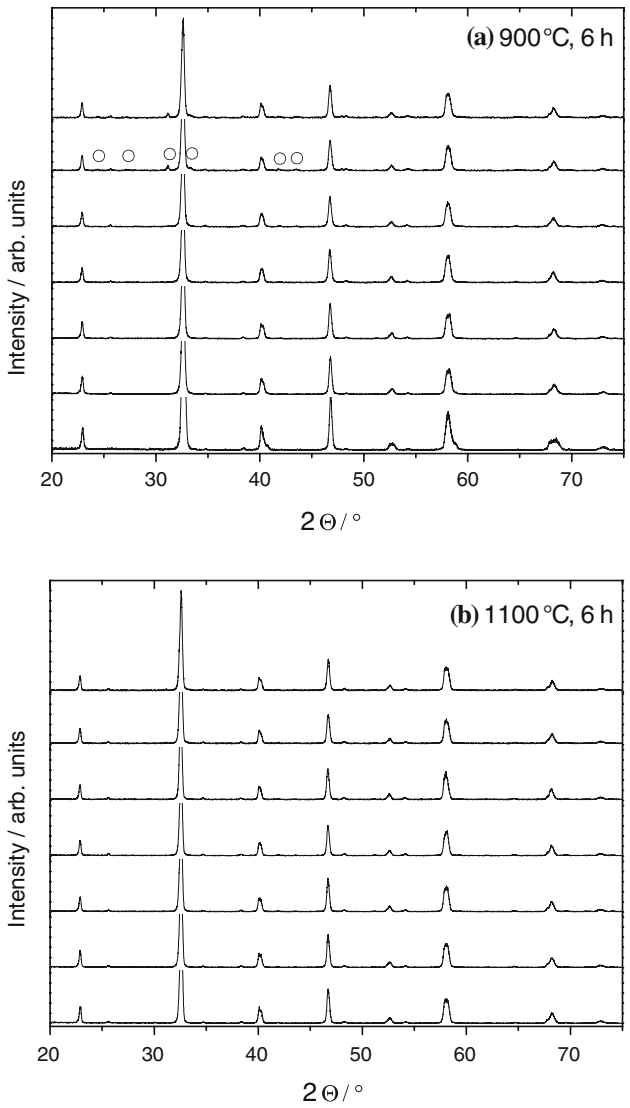

Fig. 3 XRD patterns of $LaMn_{0.75-x}Co_{0.25-x}Cu_{2x}O_{3-\delta}$ ($x = 0$, 0.025, 0.05, 0.1, 0.15, 0.2, and 0.25, from bottom to top) after heat treatment at **a** 900 °C or **b** 1100 °C for 6 h. The patterns show the formation of a single-phase orthorhombic perovskite structure (P_{or}), except in two cases ($x = 0.2$ and 0.25 calcined at 900 °C) which additionally contain the La_2CuO_4 phase as indicated by *open circles*

were obtained for $x \leq 0.15$. For $x \geq 0.2$, La_2CuO_4 was observed as minor phase. At 1100 °C, however, all powders crystallized as single-phase orthorhombic perovskites (Fig. 3). The observed crystalline phases after calcination at 900 or 1100 °C for each composition are listed in Table 1. In comparison to the Co-rich series ($LaMn_{0.25-x}Co_{0.75-x}Cu_{2x}O_{3-\delta}$), Cu apparently has a higher solubility in the Mn-rich series ($LaMn_{0.75-x}Co_{0.25-x}Cu_{2x}O_{3-\delta}$). This trend is in agreement with previous crystallographic studies on the $LaCo_{1-a}Cu_aO_3$ series and $LaMn_{1-a}Cu_aO_3$ series [11–13], and can be explained by the fact that Mn ions can easily change their valence from +3 to +4 as Cu^{2+} ions are introduced into the perovskite lattice for the charge compensation, while only Co^{3+} ions exist in these compounds [13].

The lattice parameters of the series $LaMn_{0.75-x}Co_{0.25-x}Cu_{2x}O_{3-\delta}$ do not vary significantly with increasing Cu content (Fig. 2b). Only the lattice parameter c increases very smoothly up to $x = 0.15$. The nearly constant lattice parameters can be understood, when the substitution with Cu is described in Kröger–Vink notation as

$$2\ Mn_{Mn}^{\times} = Cu_{Mn}' + Mn_{Mn}^{\bullet} \quad (1)$$

and the two Mn^{3+} ions with $r_{Mn^{3+}} = 0.645$ Å are replaced by a smaller and a bigger ion, i.e. Mn^{4+} ($r_{Mn^{4+}} = 0.53$ Å) and Cu^{2+} ($r_{Cu^{2+}} = 0.73$ Å), respectively [19], with nearly the same mean ionic radius as $r_{Mn^{3+}}$.

Thermal expansion

The thermal expansion behavior of $LaMn_{0.25-x}Co_{0.75-x}Cu_{2x}O_{3-\delta}$ is shown in Fig. 4 and the corresponding thermal expansion coefficients (TECs) between 30 and 800 °C are presented in Fig. 5. Between $0 < x < 0.15$, the TECs vary only slightly between 18.4 and 18.8 $\times 10^{-6}$ K^{-1} and a smooth maximum is observed with 19.6 $\times 10^{-6}$ K^{-1} for $LaMn_{0.2}Co_{0.7}Cu_{0.1}O_{3-\delta}$. Only the two end members with $x = 0.2$ and 0.25 show a reduced TEC, which is probably due to the increased amounts of secondary phases (L2C2 and L2C). This assumption is supported by the expansion curves at high temperatures. Whereas the sample with $x = 0.15$ shows a small bending downwards, the two samples with $x = 0.2$ and 0.25 show an abrupt shrinkage starting at 980–1000 °C. Earlier studies on $La_{0.8}Sr_{0.2}CuO_{2.4+\delta}$ revealed a small weight loss at this temperature due to the release of oxygen and the reduction of Cu^{3+} to Cu^{2+} [20]. The formation of a L2C phase with stoichiometric oxygen content, i.e. $La_2(Mn,Co,Cu)O_4$, might explain

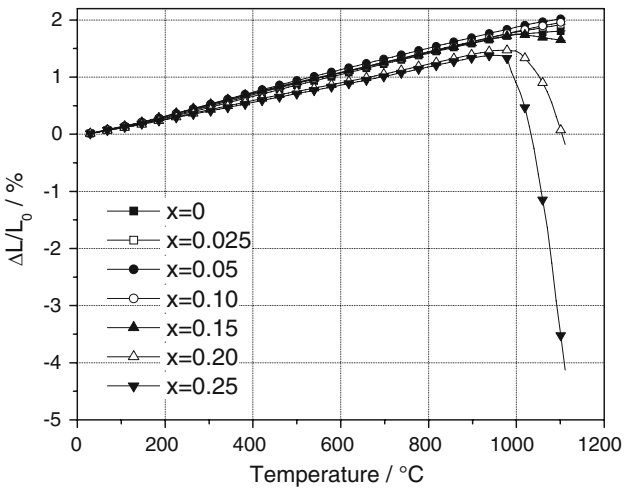

Fig. 4 Thermal expansion curves for the $LaMn_{0.25-x}Co_{0.75-x}Cu_{2x}O_{3-\delta}$ series

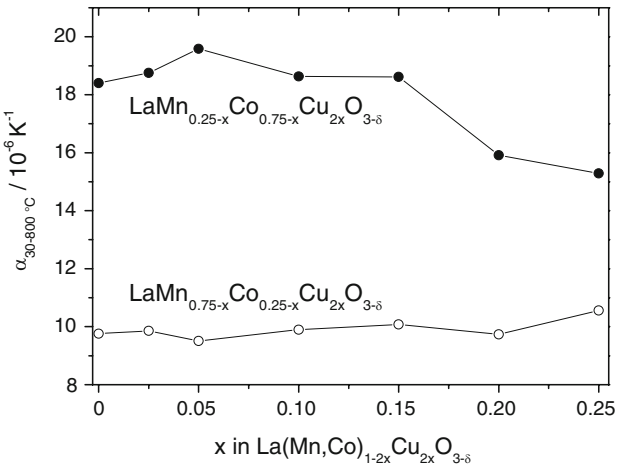

Fig. 5 Thermal expansion coefficients between 30 and 800 °C for both $LaMn_{0.25-x}Co_{0.75-x}Cu_{2x}O_{3-\delta}$ and $LaMn_{0.75-x}Co_{0.25-x}Cu_{2x}O_{3-\delta}$ as a function of Cu content

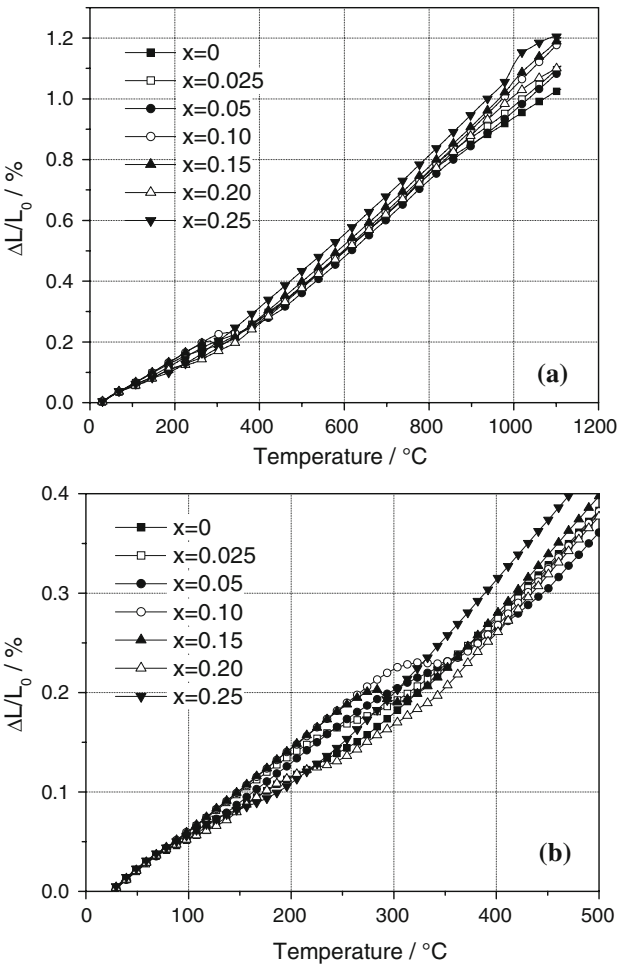

Fig. 6 **a** Thermal expansion curves for the $LaMn_{0.75-x}Co_{0.25-x}Cu_{2x}O_{3-\delta}$ series. **b** Enlarged low-temperature region of the expansion curves

the small deviation from the linear expansion curve for the sample with $x = 0.15$. In the other two cases, however, this reaction seems to be accompanied with a partial melting of the samples. An eutectic temperature of $\sim$1025 °C was reported in the $La_2Cu_2O_5$–La_2CuO_4–CuO system [21], resulting in a softening of the bars and shrinkage due to the low pressure of the push-rod of the dilatometer.

The thermal expansion curves of $LaMn_{0.75-x}Co_{0.25-x}Cu_{2x}O_{3-\delta}$ appear rather uniform at first sight (Fig. 6a) and the TECs vary only slightly between 9.5 and 10.6 $\times$ 10^{-6} K^{-1} without any dependence on the copper content (Fig. 5). It is interesting to note that no pronounced maximum in TEC was observed for either series, whereas for $La(Mn_{0.5}Co_{0.5})_{1-x}Cu_xO_{3-\delta}$ a systematic increase and decrease of TEC with a maximum at $x = 0.4$ was found [14]. In addition, it is worth mentioning that no shrinkage was caused by partial melting and that the Mn-rich perovskites possessed higher temperature stability than the Co-rich samples.

All expansion curves in Fig. 6a show a slope change at about 300 °C. An enlarged view of this low-temperature region is presented in Fig. 6b. For most of the samples, a smooth slope change was observed. For $x = 0.1$ and 0.15, however, a pronounced horizontal S-shape was measured. These irregularities from linear expansion are often related to phase transitions. Since all of the samples of the $LaMn_{0.75-x}Co_{0.25-x}Cu_{2x}O_{3-\delta}$ series crystallized as orthorhombic perovskites, it can be assumed that they transformed to a perovskite with higher symmetry at elevated temperatures, as is the case for $(La,Sr)(Co,Fe)O_3$ perovskites [22]. Apart from the degree of non-linearity among the different compositions, the temperature dependence of the phase transition was analyzed in more detail by generating the derivatives of the expansion curves and determining the temperatures for the onset, minimum and end of the slope change reflecting the beginning, maximum rate and end of the phase transition (Fig. 7). Depending on the Cu content, the phase transition occurred at 200 °C for $LaMn_{0.75}Co_{0.25}O_{3-\delta}$, shifted to about 350 °C for $LaMn_{0.65}Co_{0.15}Cu_{0.2}O_{3-\delta}$ and dropped back to about 150–200 °C for $LaMn_{0.5}Cu_{0.5}O_{3-\delta}$. In the derivative curves for the samples with $x = 0$, 0.2 and 0.25, a second minimum was found. In these cases, it is not clear whether this signal can be attributed to an additional phase change, a stepwise phase transition or the influence of inhomogeneities within the samples. It should be noted that the temperature width of the phase transition varied between 100 and 200 °C, indicating a compositional variation between different grains.

Electrical conductivity

The electrical conductivity of $LaMnO_{3-\delta}$ showed a semiconducting temperature dependence and can generally be

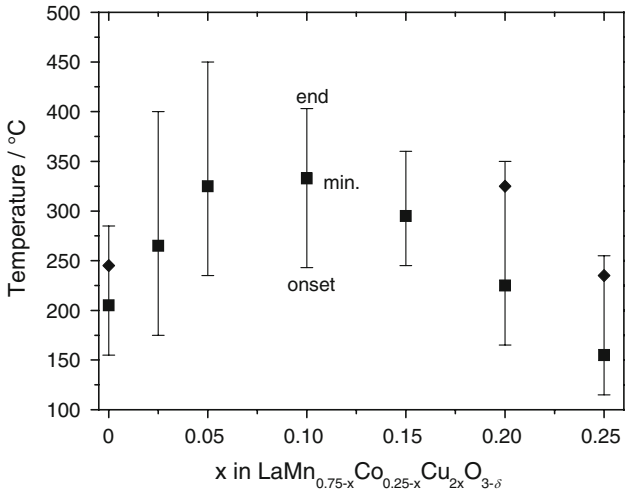

Fig. 7 Phase transition temperatures for $LaMn_{0.75-x}Co_{0.25-x}Cu_{2x}O_{3-\delta}$ extracted from derivatives of the thermal expansion curves in Fig. 6b. For $x = 0$, 0.20 and 0.25, two minima in the derivatives of the expansion curves were observed (indicated by *filled diamonds*)

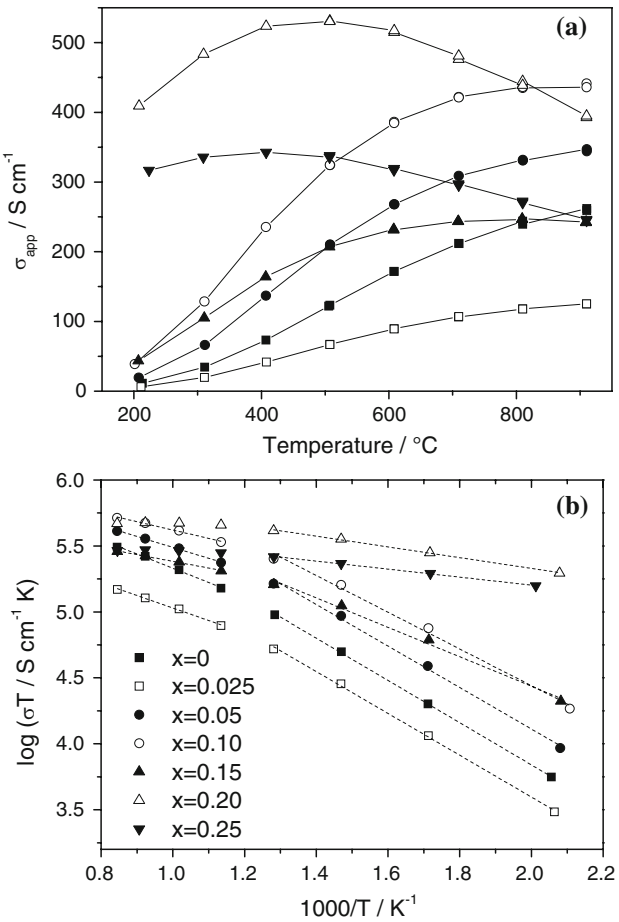

Fig. 8 **a** Measured apparent conductivity (σ_{app}) versus temperature (T) and **b** log σT versus 1000/T for $LaMn_{0.25-x}Co_{0.75-x}Cu_{2x}O_{3-\delta}$. The electrical conductivity data were not corrected with the sample density. Symbols in **b** belong to the same samples in **a**. *Dashed lines* in **b** are fitted straight lines for the calculation of activation energies

explained by the hopping of p-type small polarons [23]. On the contrary, the conductivity of $LaCoO_{3-\delta}$ showed a semiconducting behavior at lower temperatures and a metallic behavior at higher temperatures [24, 25]. In general, the band gap between valence and conduction band is narrowing along the transitions metals from Cr to Ni [26] which explains the different temperature dependence of conductivity of the perovskites (see discussion further below). In the present work, all compositions except two showed semiconducting behavior in the temperature range studied (100–900 °C). The two exceptions, $LaMn_{0.25-x}Co_{0.75-x}Cu_{2x}O_{3-\delta}$ with $x = 0.20$ and $x = 0.25$, showed metallic behavior at higher temperatures (Fig. 8a), although the sample with $x = 0.25$ contains 22 wt% L2C2 having semiconducting temperature dependence [14]. Therefore, we treated all samples by a hopping mechanism and considered the small impurities in the samples of $LaMn_{0.25-x}Co_{0.75-x}Cu_{2x}O_{3-\delta}$ with $x \leq 0.2$ (see Table 1) as negligible contribution to the total conductivity, whereas the L2C2 content in $LaMn_{0.25-x}Co_{0.75-x}Cu_{2x}O_{3-\delta}$ with $x = 0.25$ seems to have a significant contribution to the total conductivity (see below). The temperature dependence of electrical conductivity through the hopping mechanism can be expressed according to [23] by

$$\sigma = A/T \exp(-E_a/kT) \quad (2)$$

where A is a material constant containing the carrier concentration term; E_a is the activation energy for hopping conduction; k is Boltzman's constant; T is the absolute temperature. The plot of log σT versus $1/T$ for $LaMn_{0.25-x}Co_{0.75-x}Cu_{2x}O_{3-\delta}$ and $LaMn_{0.75-x}Co_{0.25-x}Cu_{2x}O_{3-\delta}$ is

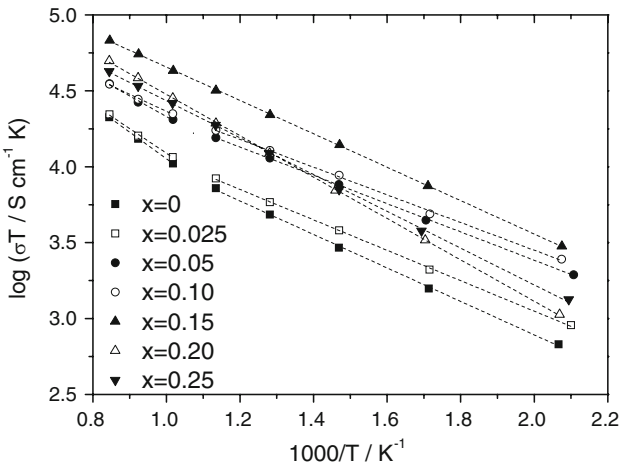

Fig. 9 Log σT versus 1000/T for $LaMn_{0.75-x}Co_{0.25-x}Cu_{2x}O_{3-\delta}$. The electrical conductivity was not corrected with sample density. *Dashed lines* are fitted straight lines for the calculation of activation energies

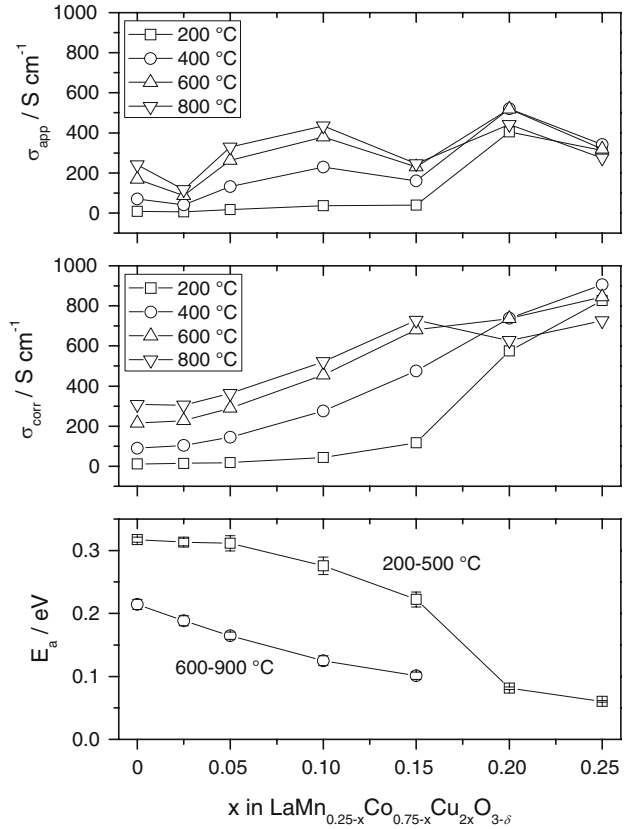

Fig. 10 Apparent and corrected electrical conductivity (σ_{app} and σ_{corr}) at 200, 400, 600 and 800 °C as well as activation energies for $LaMn_{0.25-x}Co_{0.75-x}Cu_{2x}O_{3-\delta}$ as a function of Cu content. The relative densities of the samples are 89, 69, 96, 92, 67, 85 and 69% for $x = 0$, 0.025, 0.05, 0.1, 0.15, 0.2, and 0.25, respectively

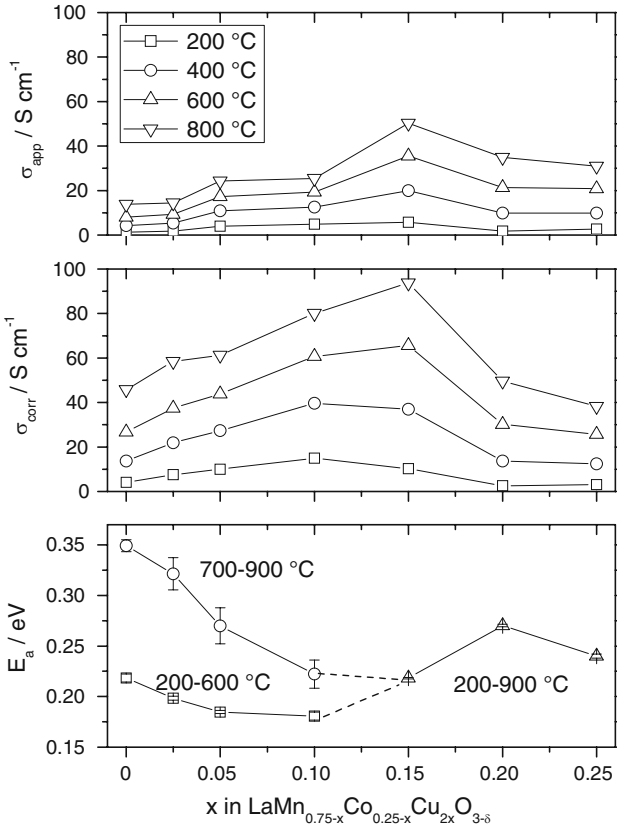

Fig. 11 Apparent and corrected electrical conductivity (σ_{app} and σ_{corr}) at 200, 400, 600, and 800 °C as well as activation energies for $LaMn_{0.75-x}Co_{0.25-x}Cu_{2x}O_{3-\delta}$ as a function of Cu content. The relative densities of the samples are 65, 62, 70, 66, 77, 85, and 90% for $x = 0$, 0.025, 0.05, 0.1, 0.15, 0.2, and 0.25, respectively

shown in Figs. 8b and 9, respectively. It can be seen that linear or nearly linear behavior was observed for both compositional series.

From the slopes of the straight lines in the plots of log σT versus $1/T$, the apparent activation energies can be calculated, as shown in Figs. 10 and 11. For $LaMn_{0.25-x}Co_{0.75-x}Cu_{2x}O_{3-\delta}$ with $x \leq 0.15$, the plot can be fitted with two segments of straight lines with different slopes at the lower temperature range (200–500 °C) and the higher temperature range (600–900 °C). For $LaMn_{0.25-x}Co_{0.75-x}Cu_{2x}O_{3-\delta}$ with $x = 0.20$ and 0.25, the data points at the higher temperature range deviate too much from the linear behavior, so that only the data points at the lower temperature range were fitted. For $LaMn_{0.75-x}Co_{0.25-x}Cu_{2x}O_{3-\delta}$ with $x \leq 0.10$, two linear regions were found at 200–600 °C and 700–900 °C. For $LaMn_{0.75-x}Co_{0.25-x}Cu_{2x}O_{3-\delta}$ with $x \geq 0.15$, all data points can be fitted with a single straight line. Figure 10 shows that the activation energies for the $LaMn_{0.25-x}Co_{0.75-x}Cu_{2x}O_{3-\delta}$ series at both lower and higher temperature range decrease monotonously with the Cu content. The activation energies at the lower temperature range are higher (0.32–0.22 eV from $x = 0$ to $x = 0.15$) than those at the higher temperature range (0.21–0.10 eV for the same compositional range). In contrast, the activation energies for the $LaMn_{0.75-x}Co_{0.25-x}Cu_{2x}O_{3-\delta}$ series first decrease and then increase with the Cu content, as shown in Fig. 11. The minimum occurs at $x = 0.10$ for the lower temperature branch and at $x = 0.15$ for the higher temperature branch. In addition, the activation energies at the lower temperature range are lower (0.22–0.18 eV from $x = 0$ to $x = 0.10$) than those at the higher temperature range (0.35–0.22 eV for the same compositional range).

The dependence of the isothermal electrical conductivity on the Cu content for $LaMn_{0.25-x}Co_{0.75-x}Cu_{2x}O_{3-\delta}$ and $LaMn_{0.75-x}Co_{0.25-x}Cu_{2x}O_{3-\delta}$ is shown in Figs. 10 and 11, respectively. It should be noted that the sintered samples with different compositions have different relative densities ranging from 62 to 96%. In order to compare the bulk properties of samples with different compositions, the influence of the sample porosity must be taken into account. Here the as-measured apparent conductivity data were corrected with the sample density using an empirical equation according to Tagawa et al. [27]:

$$\sigma_{app}/\sigma_{corr} = 2(d_{rel}/100 - 0.5) \quad (3)$$

where σ_{corr} is the corrected electrical conductivity, σ_{app} the measured apparent conductivity, and d_{rel} the relative density (%). In Figs. 10 and 11, both the as-measured apparent conductivity and the corrected conductivity are shown as a function of Cu content. For the $LaMn_{0.25-x}Co_{0.75-x}Cu_{2x}O_{3-\delta}$ series, no clear trend was found for the apparent conductivity due to interference from the sample densities. The corrected conductivity, however, increased with the Cu content at temperatures of below 600 °C. At higher temperatures, the conductivity began to decrease at $x = 0.20$, which can be correlated to the appearance of metallic conduction at these temperatures. In addition, the apparent conductivity of the sample with $x = 0.2$ was higher than the sample with $x = 0.25$. Besides the porosity, here the L2C2 phase may also have an influence, because this phase has an electrical conductivity of only $\approx$ 10 S/cm at 800 °C [14] leading to reduced conductivity values. Therefore, the compound $LaCo_{0.5}Cu_{0.5}O_{3-\delta}$ should be regarded as a composite of $La_2Cu_2O_5$ and Cu-substituted $LaCoO_3$.

For the $LaMn_{0.75-x}Co_{0.25-x}Cu_{2x}O_{3-\delta}$ series, both the apparent and corrected conductivity show similar profiles, i.e. a conductivity maximum is observed at $x = 0.10$ at the lower temperature range (<400 °C) or at $x = 0.15$ at the higher temperature range (>400 °C). From Figs. 10 and 11, it appears that lower activation energies correspond to higher electrical conductivity. In addition, compared to the Mn-rich series ($LaMn_{0.75-x}Co_{0.25-x}Cu_{2x}O_{3-\delta}$), the Co-rich series ($LaMn_{0.25-x}Co_{0.75-x}Cu_{2x}O_{3-\delta}$) shows significantly higher electrical conductivity, which is consistent with the fact that $LaCoO_3$-based perovskites have a much higher electrical conductivity than $LaMnO_3$-based perovskites [1, 10, 22]. The higher electrical conductivity of the cobaltites is due to the narrower band gap and the shifted Fermi level in the electronic band structure [26]. Although both series contain Mn and Co on the B-site of the perovskite structure, the electrical conductivity of $LaMn_{0.75}Co_{0.25}O_{3-\delta}$ and $LaMn_{0.25}Co_{0.75}O_{3-\delta}$ reflects the electronic band structure of $LaMnO_3$ and $LaCoO_3$, respectively [26]. The addition of Cu in both series leads to a higher conductivity and lower activation energy which clearly indicates the occupation of electronic states within the band gap of valence and conduction band, either as single energy levels (low Cu concentrations) or as small narrow bands (high Cu concentrations), similar to the A-site substitution with Sr in these perovskites [26]. In the case of the Co-rich series, the band gap becomes so small that the thermal energy at elevated temperatures is sufficient to activate electrons occupying energy levels in the conduction band. As shown in Fig. 8a, the maximum conductivity of the samples with $x = 0.20$ and $x = 0.25$ was observed at 500 and 400 °C corresponding to a thermal energy of RT = 6.43 and 5.56 kJ/mol (i.e. 0.067 and 0.058 eV), respectively ($R = 8.3144$ J K^{-1} mol^{-1}). These values correspond very well with the measured activation energies at lower temperatures of these two samples (0.081 and 0.060 eV, cf. Fig. 10) and indicate a thermally activated electronic conduction in Cu-rich perovskite materials similar to Ni-based peovskites ($LaNiO_3$, $LaNi_{1-x}Fe_xO_3$) [26, 28–30].

Conclusions

Two series of perovskite oxides ($LaMn_{0.25-x}Co_{0.75-x}Cu_{2x}O_{3-\delta}$ and $LaMn_{0.75-x}Co_{0.25-x}Cu_{2x}O_{3-\delta}$ with $x = 0$, 0.025, 0.05, 0.1, 0.15, 0.2, and 0.25) in the quasi-ternary system $LaMnO_3$–$LaCoO_3$–"$LaCuO_3$" have been investigated in terms of crystal structure, thermal expansion and electrical conductivity. In comparison to the Co-rich series ($LaMn_{0.25-x}Co_{0.75-x}Cu_{2x}O_{3-\delta}$), the Mn-rich series ($LaMn_{0.75-x}Co_{0.25-x}Cu_{2x}O_{3-\delta}$) can tolerate higher concentrations of Cu in the lattice without forming Cu-containing secondary phases. After calcination at 1100 °C, all compositions in the Mn-rich series crystallized as single-phase orthorhombic perovskites showing no significant variation of the lattice parameters. The Co-rich series showed a much higher thermal expansion coefficient and electrical conductivity than the Mn-rich series. Irregularities in the thermal expansion curves indicated phase transitions at 150–350 °C for the Mn-rich series, while partial melting occurred at 980–1000 °C for the Co-rich series with higher Cu contents. For both series, the influence of the Cu content on the thermal expansion coefficient is not as pronounced as on the electrical conductivity. The electrical conductivity of the Co-rich series increased with the Cu content at temperatures below 600 °C. At higher temperatures, metallic conduction was observed for compositions with $x > 0.15$. For the Mn-rich series, however, a conductivity maximum was observed at $x = 0.10$-0.15, and all compositions showed semiconducting behavior.

Acknowledgements The authors thank P. Lersch (deceased) and M. Ziegner for XRD measurements, A. Hilgers and M.-T. Gerhards for dilatometric measurements, and H. Lippert and N. Merki (FZJ-ZCH) for chemical analyses.

References

1. Kharton VV, Yaremchenko AA, Naumovich EN (1999) J Solid State Electrochem 3:303 (and references therein)
2. Narasimhan V, Keer HV, Chakrabarty DK (1985) Phys Status Solidi A 89:65
3. De Souza RA, Kilner JA (1998) Solid State Ion 106:175
4. Seiyama T (1992) Catal Rev Sci Eng 34:281
5. Banerjee S, Choudhary VR (2000) Proc Indian Acad Sci (Chem Sci) 112:535

6. von Helmholt R, Wecker J, Holzapfel B, Schultz L, Samwer K (1993) Phys Rev Lett 71:2331
7. Urushibara A, Moritomo Y, Arima T, Asamitsu A, Kido G, Tokura Y (1995) Phys Rev B 51:14103
8. Radwański RJ, Ropka Z (2000) Physica B 281&282:507
9. Tietz F (1999) In: Vincenzini P (ed) Proc. 9th CIMTEC-World ceramic congress and forum on new materials, vol 24. Techna Publishers S.r.l., Faenza, Italy, pp 61–70
10. Petric A, Huang P, Tietz F (2000) Solid State Ion 135:719
11. Tikhonova IL, Zuev AYu, Petrov AN (1998) Russ J Phys Chem 72:1625
12. Tikhonova IL, Bakhtin AV, Zuev AYu, Petrov AN (1999) Russ J Phys Chem 73:365
13. Porta P, De Rossi S, Faticanti M, Minelli G, Pettiti I, Lisi L, Turco M (1999) J Solid State Chem 146:291
14. Tietz F, Schmidt A, Zahid M (2004) J Solid State Chem 177:745
15. Demazeau G, Parent C, Pouchard M, Hagenmuller P (1973) Mater Res Bull 7:913
16. Bringley JF, Scott BA, La Placa SJ, McGuire TR, Mehran F (1993) Phys Rev B 47:15269
17. Pechini MP (1967) US Patent 3,330,697
18. Tietz F, Arul Raj I, Jungen W, Stöver D (2001) Acta Mater 49:803
19. Shannon RD (1976) Acta Crystallogr A32:751
20. Zahid M, Arul Raj I, Fischer W, Tietz F, Serra Alfaro JM (2006) Solid State Ion 177:3205
21. Skakle JMS, West AR (1994) J Am Ceram Soc 77:2199
22. Tai L-W, Nasrallah MM, Anderson HU, Sparlin DM, Sehlin SR (1995) Solid State Ion 76:259, 273
23. Mizusaki J, Yonemura Y, Kamata H, Ohyama K, Mori N, Takai H, Tagawa H, Dokiya M, Naraya K, Sasamoto T, Inaba H, Hashimoto T (2000) Solid State Ion 132:167
24. Thornton G, Tofield BC, Williams DE (1982) Solid State Commun 44:1213
25. Mizusaki J, Tabuchi J, Matsuura T, Yamauchi S, Fueki K (1989) J Electrochem Soc 136:2082
26. Sarma DD, Chainani A (1994) J Solid State Chem 111:208
27. Tagawa H, Mizusaki J, Arai Y, Kuwayama Y, Tsutiya S, Takeda T, Sesido S (1990) Denki Kagaku oyobi Kogyo Butsuri Kagaku 58:512
28. Rajeev KP, Shivashankar GV, Raychaudhuri AK (1991) Solid State Commun 79:591
29. Sreedhar K, Honig JM, Darwin M, McElfresh M, Shand PM, Xu J, Crooker BC, Spalek J (1992) Phys Rev B 46:6382
30. Chiba R, Yoshimura F, Sakurai Y (1999) Solid State Ion 124:281